



Published in final edited form as:

*Nat Nanotechnol.* 2019 October ; 14(10): 974–980. doi:10.1038/s41565-019-0539-2.

## A biodegradable nanocapsule delivers a Cas9 ribonucleoprotein complex for *in vivo* genome editing

Guojun Chen<sup>1,2,#</sup>, Amr A. Abdeen<sup>2,#</sup>, Yuyuan Wang<sup>1,2,#</sup>, Pawan K. Shahi<sup>3</sup>, Samantha Robertson<sup>4</sup>, Ruosen Xie<sup>1,2</sup>, Masatoshi Suzuki<sup>4,5</sup>, Bikash R. Pattnaik<sup>3,6</sup>, Krishanu Saha<sup>2,5,\*</sup>, Shaoqin Gong<sup>1,2,5,7,\*</sup>

<sup>1</sup>Department of Materials Science and Engineering, University of Wisconsin–Madison, Madison, WI 53715, USA.

<sup>2</sup>Wisconsin Institute for Discovery, University of Wisconsin–Madison, Madison, WI 53715, USA.

<sup>3</sup>Department of Pediatrics, University of Wisconsin - Madison, Madison, WI 53706, USA.

<sup>4</sup>Department of Comparative Biosciences, University of Wisconsin – Madison, Madison, WI 53706, USA

<sup>5</sup>Department of Biomedical Engineering, University of Wisconsin–Madison, Madison, WI 53715, USA.

<sup>6</sup>Department of Ophthalmology and Visual Sciences, University of Wisconsin – Madison, Madison, WI 53706, USA

<sup>7</sup>Department of Chemistry, University of Wisconsin–Madison, Madison, WI 53715, USA.

### Abstract

Delivery technologies for the CRISPR-Cas9 gene editing system often require viral vectors, which pose safety concerns for therapeutic genome editing<sup>1</sup>. Alternatively, cationic liposomal components or polymers can be used to encapsulate multiple CRISPR components into large particles (typically >100 nm diameter); however, such systems are limited by variability in loading of the cargo. Here, we report the design of customizable synthetic nanoparticles for the delivery of Cas9 nuclease and a single-guide RNA (sgRNA), enabling controlled stoichiometry of CRISPR components and limiting possible safety concerns *in vivo*. We describe the synthesis of a thin

Users may view, print, copy, and download text and data-mine the content in such documents, for the purposes of academic research, subject always to the full Conditions of use:[http://www.nature.com/authors/editorial\\_policies/license.html#terms](http://www.nature.com/authors/editorial_policies/license.html#terms)

\*Correspondence should be addressed to KS (ksaha@wisc.edu) and SG (shaoqingong@wisc.edu).

#. These authors contributed equally.

#### Author Contributions

G.C., A.A.A., Y.W., K.S., and S.G. conceived and designed the project; G.C., A.A.A., Y.W., R.X., M.S., S.R., and P.K.S. performed the experiments; all authors analyzed the data; and G.C., A.A.A., Y.W., P.K.S., B.R.P., M.S., K.S., and S.G. co-wrote the paper.

#### Competing Financial Interests

G.C., A.A.A., Y.W., R.X., K.S., and S.G. have filed a patent application on this work.

#### Additional information

Supplementary information is available in the online version of the paper. Reprints and permission information is available online at [www.nature.com/reprints](http://www.nature.com/reprints). Correspondence and requests for materials should be addressed to KS and SG.

#### Data Availability

The data that support the plots within this paper and other findings of this study are available from the corresponding authors upon reasonable request.

glutathione (GSH)-cleavable covalently-crosslinked polymer coating, called a nanocapsule (NC), around a pre-assembled ribonucleoprotein (RNP) complex between a Cas9 nuclease and a sgRNA. The NC is synthesized by acrylate-based polymerization, has a hydrodynamic diameter of 25 nm, and can be customized via facile surface modification. NCs efficiently generate targeted gene edits *in vitro* without any apparent cytotoxicity. Furthermore, NCs produce robust gene editing *in vivo* in murine retinal pigment epithelium (RPE) tissue and skeletal muscle following local administration. This customizable NC nanoplatform efficiently delivers CRISPR RNP complexes for *in vitro* and *in vivo* somatic gene editing.

Cas9 RNP is an attractive nonviral formulation for CRISPR-mediated gene editing due to its quick DNA cleavage activity, low off-target effects<sup>1, 2</sup>, low risk of insertional mutagenesis, and ease of production<sup>3</sup>. Furthermore, RNPs do not rely on transcriptional or translational cellular machinery for precise enzymatic gene editing activity, nor carry any long nucleic acids or viral based approaches that could integrate into the genome. However, existing nonviral strategies for the delivery of Cas9 RNP face a number of challenges<sup>4, 5, 6, 7</sup>, such as high cytotoxicity, poor *in vivo* stability, large particle sizes, lack of specific tissue/cell-targeting abilities, variable loading of the RNP cargo, and potential immunogenicity. These challenges limit the application of RNPs for gene editing *in vitro*, and especially *in vivo* where chemically-defined stable and off-the-shelf formulations could be critical for translational somatic gene editing applications<sup>1</sup>.

We sought to develop a customizable and efficient nanoplatform to deliver Cas9 RNP complexes for both *in vitro* and *in vivo* applications. Our design criteria include: high RNP loading content; small nanoparticle sizes; controllable stoichiometry; excellent stability; endosomal escape capability; efficient RNP release once inside the cytosol; and, amenability to surface modifications. As shown in Fig. 1a, because the RNP exhibits heterogeneous surface charges on the Cas9 protein and sgRNA<sup>5</sup>, we posited that a mixture of cationic and anionic acrylate monomers (*i* and *ii*, respectively) could form a coating around the RNP through electrostatic interactions. An imidazole-containing monomer (*iii*), GSH-degradable crosslinker (*iv*), acrylate mPEG (*v*), and acrylate PEG conjugated ligands (*vi*) can also be attracted to the surface of the RNP complex *via* hydrogen bonding and van der Waals interactions<sup>8, 9</sup>. After monomer coating, subsequent *in situ* free-radical polymerization<sup>8, 9, 10</sup> was initiated to form a covalently linked, yet glutathione (GSH)-cleavable NC around RNP. The integration of the imidazole-containing acrylate monomer can facilitate endosomal escape of the NCs owing to the proton sponge effect of imidazole groups<sup>11</sup>. NCs were crosslinked with a GSH-cleavable linker, N,N'-bis(acryloyl)cystamine, which can be degraded in GSH-rich environments such as the cytosol (2–10 mM<sup>12, 13</sup>), thereby enabling the release of RNPs within the cytosol (Fig. 1b). The RNPs can then enter the nucleus, which may be further facilitated by nuclear localization signals (NLSs) fused to the recombinant Cas9 protein<sup>14</sup>. The outer water-soluble PEG shell adds flexibility to conjugate functional moieties, such as targeting ligands, cell penetrating peptides (CPPs), or imaging probes.

To find optimal monomer stoichiometry for efficient cellular transfection, the amounts of various monomers were adjusted systematically as summarized in Fig. 1c. Several critical

factors were investigated, including the anionic/cationic monomer ratio, the amounts of the imidazole-containing monomer and crosslinker, and the mass ratio between the NC and RNP. The functionality of NCs with different formulations were tested on a human embryonic kidney (HEK) cell line with an H2B-mCherry transgene (red fluorescence localized to each nucleus)<sup>15, 16</sup>. Using a suitable sgRNA targeting the mCherry transgene, successful gene editing results in a loss of red fluorescence that is easily detectable through flow cytometry.

It is essential to use both cationic and anionic monomers due to the heterogeneous charge distribution of RNP (Fig. 1c). Pure cationic or anionic monomer formulations exhibited negligible gene editing, likely due to incomplete coating of the RNP. The ratios of anionic and cationic monomers also affected the gene editing efficiency. The formulation containing a mixture of cationic and anionic monomers at an anionic/cationic ratio of 1:1 (the optimal formulation) exhibited the highest gene editing levels (Fig. 1c). The amounts of the imidazole monomer and biodegradable crosslinker were also critical for efficient gene editing (Fig. 1c). Without imidazole-containing monomers, NCs induced relatively low levels of gene editing. Higher editing efficiencies were achieved with increases in imidazole-containing monomers. Also, at a low crosslinker amount, no gene editing was observed, likely due to unsuccessful formation of NCs. With sufficient amounts of crosslinker, similar gene editing capabilities were detected, suggesting a minimum required threshold for crosslinker to successfully form NCs. Higher crosslinker concentrations caused a reduction in gene editing efficiency. Furthermore, NCs formed by a non-biodegradable crosslinker (bisacrylamide) showed no editing, indicating that NCs must be biodegradable in order to produce gene edits. The mass ratios between the NC and RNP impacted gene editing efficiencies, as sufficient acrylate monomers are needed to form a polymer coating around RNP. NCs with a low NC:RNP ratio (50% of the optimal formulation) exhibited gene editing efficiencies barely above the baseline (Fig. 1c). On the other hand, excessive polymer coating over RNP (200% of the optimal formulation) also reduced the editing efficiency, likely attributed to the fact that NCs with a thicker polymeric shell require a longer time to fully degrade and release RNP to function. Collectively, the critical range for functional encapsulation of RNPs was determined after systematically titrating all key components, and the optimal NC formulation (referred to as NC subsequently) was selected for further study. The RNP loading level of the optimal NC was 40%. Fig. 1d shows a transmission electron microscope image of uniformly sized NCs with an average diameter of 16 nm. The average hydrodynamic diameter of NCs was 25 nm measured by dynamic light scattering (Fig. 1e). The zeta potential of NCs was relatively neutral (i.e., -4 mV), indicating that the net negative charge of the RNP was masked by the NC (Fig. 1f).

The stability of NCs before cell internalization is critical for successful genome editing. Although the GSH-degradable NCs are expected to remain stable in the extracellular spaces and circulation (GSH concentration: 0.001–0.02 mM)<sup>12, 13</sup>, their stability was systematically tested because the degradability of disulfide bonds in different polymers can differ<sup>17</sup>. To determine at which GSH concentration NCs remain stable and functional, cell culture media containing different concentrations of GSH were used during NC treatment. The gene editing efficiency of NCs did not change at a GSH concentration of 0.1 mM or lower, indicating that NCs were stable and functional at a GSH concentration at least up to 0.1 mM

(Fig. 2a). At a GSH concentration of 1 mM or higher, the gene editing efficiency decreased, suggesting that NCs were disrupted before cell internalization. This also implies that NCs are GSH-responsive and RNP cargo can be efficiently released from NCs in the GSH-rich cytosol (2–10 mM).

We examined the subcellular localization of the RNP cargo in HEK cells *in vitro*. As shown in Fig. 2b, after 6 h incubation, most of RNP (red fluorescence) and endosomes (green fluorescence) were not overlapping, indicating that RNPs were capable of escaping from the endosomes.

We then compared the *in vitro* gene editing functionality of NCs with Lipofectamine-based delivery vehicles, (e.g., Lipofectamine 2000 and Lipofectamine CRISPRMAX), the state-of-the-art, commercially available transfection agents for RNP delivery. Lipofectamine delivery systems were also systemically optimized (Fig. S1), where Lipofectamine 2000 with 0.75  $\mu$ l per well in the 96-well plate exhibited the highest gene editing efficiency, which was used for the following study (denoted as Lipo). Unencapsulated RNP treatment was included since RNP itself shows some cell penetrating capability, likely conferred by the positively-charged NLSs<sup>18</sup>. Compared to the untreated control, RNP alone induced only  $1.6 \pm 0.5\%$  editing above the background levels, which was significantly lower than that delivered by either Lipo (i.e.,  $60.1 \pm 1.7\%$ ), or NC (i.e.,  $79.1 \pm 0.6\%$ ), where NCs exhibited the highest editing efficiency (Fig. 2c). Moreover, NCs did not cause apparent cytotoxicity in HEK cells (<6% cell death), while consistent with other studies, Lipo exhibited significant cytotoxicity when it was used to deliver the same amount of RNP (i.e., ~25% cell death, Fig. 2d). Importantly, NCs could be freeze-dried and reconstituted at high concentrations (~5  $\mu$ g/ $\mu$ L) while retaining potency (>90%), unlike many liposomal delivery agents that lose stability upon freeze-drying<sup>19</sup> (Fig. 2e and Fig. S1).

To demonstrate the versatility of NC surface modification, we first functionalized NCs with CPPs (i.e., NC-CPP, Fig. 3a), which are known to enhance the cellular uptake efficiency of nanoparticles. CPPs (or the targeting ligand, all-trans retinoic acid (ATRA), used in the following *in vivo* experiments) were incorporated onto the distal ends of a higher molecular weight PEG (i.e., 2 kDa). The use of longer PEGs could potentially reduce the steric hindrance from the surrounding mPEG segments (i.e., 480 Da), allowing for better targeting or penetrating capabilities<sup>20</sup>. Detailed polymer and NC characterizations are shown in the Supplementary Information (Figs. S2 and S3 and Table S1). As expected, CPP conjugation on NCs significantly enhanced (~1.5 fold) their level of cellular uptake (Fig. S4). Moreover, when loaded with RNP targeting the endogenous *APP* gene, NC-CPP enhanced editing efficiency in HEK cells as well as human embryonic stem cells (hESCs), a notoriously hard-to-transfect cell type (Fig. 3). Deep sequencing of the on-target region around *APP* revealed high-efficiency editing at this endogenous locus. In HEKs, NC-CPP increased editing efficiency two-fold (Fig. 3a), while in hESCs, NC-CPP increased editing efficiency approximately three-fold (Fig. 3d). The deletion spectra (Fig. 3b–e) for both cell types contained a 5 base deletion as a frequent editing outcome in all of the samples, consistent with a previous report using this sgRNA sequence<sup>21</sup>. Together, these *in vitro* results demonstrate that decoration of the NC can enhance genome editing at an endogenous, therapeutically relevant locus without changing the types of edits produced by Cas9.

Gene editing using NCs was finally evaluated *in vivo* in the eyes and muscles of transgenic Ai14 mice (Fig. 4). All cells within Ai14 mice contain a stop cassette, comprised of three sv40 polyA transcription terminators, preventing expression of a constitutive tdTomato fluorescent reporter. tdTomato expression can be induced *via* excision of the sv40 polyA genetic elements (Fig. 4a). Successful gene editing can therefore be easily evaluated through fluorescence<sup>18</sup>. First, we evaluated gene editing within the retinal pigmented epithelium (RPE) because over two million people worldwide are affected by monogenic diseases of the eye<sup>22</sup>, and several somatic gene editing strategies are being developed for subretinal delivery<sup>23</sup>. We tested whether surface modification of the NC could affect its gene editing performance within RPE. NCs were decorated with ATRA (i.e., NC-ATRA). ATRA binds to the inter-photoreceptor retinoid-binding protein, a major protein in the inter-photoreceptor matrix that selectively transports 11-cis-retinal to photoreceptor outer segments and all-trans-retinol to the RPE<sup>24</sup>. Mice were subretinally injected with a PBS vehicle, RNP alone, NC, or NC-ATRA (Fig. 4b, c). Successful subretinal injection was indicated by a bleb formation immediately next to the RPE (Fig. S5). Twelve days post injection, enucleated eyes were whole-mounted to evaluate gene editing globally over the entire RPE tissue (Fig. 4d, e). In contrast to the *in vitro* results in HEKs as discussed previously and the *in vivo* results in muscle cells to be discussed later, where RNP alone did not induce any genome editing, unencapsulated RNP was able to induce genome editing in RPEs. This may be attributed to the inherent function of this tissue as a transport epithelium: RPE cells are involved in the movement of nutrients and waste products through bidirectional passive and active pathways<sup>25, 26</sup>. The subretinal space is a tight space that ensures fluid absorption from retina to choroid direction through the RPE layer for retina reattachment following subretinal injections, and further RPE cells are among the most actively phagocytic cells found in the body<sup>27, 28</sup>. NCs also exhibited considerable gene editing, and NC-ATRA induced significantly higher editing efficiency than other groups (Figs 4d, e). Second, we tested the activity of NCs in muscle tissue via intramuscular administration in the same mouse model (Fig. 4f). As shown in Fig. 4g and 4h, unencapsulated RNP failed to induce any genome editing in muscles, while NCs induced robust gene editing. Interestingly, strong tdTomato signals were identified in the cells within the basal lamina between muscle fibers. Because muscle satellite cells—quiescent mononucleated myogenic cells in adult muscle—are present in this region, we performed immunohistochemistry to co-stain with Pax7 (a muscle satellite cell marker) and tdTomato (RFP) in the muscle sections. Overlapping signals of Pax7 and RFP in NC-injected muscle (Fig. S6) indicated that Pax7-positive satellite cells expressed tdTomato protein. Collectively, these results demonstrated that NC formulations could produce gene edits *in vivo*, the extent of which can be further modulated by surface functionalization.

Our approach accommodates the charge heterogeneity of Cas9 RNP (~9 nm in diameter) to form covalently-linked stable, yet biodegradable, NCs. NCs were formed by coating RNPs using a mixture of monomers with distinct functions as described above. The RNP serves as the core/scaffold for the formation of the NC. The acrylate monomers are attracted to the RNP surface either electrostatically or *via* van der Waals forces and hydrogen bonding for subsequent polymerization, resulting in nearly monodispersed NCs with an average size of 16 nm in the dried state. This chemically defined strategy, therefore, has a fixed

stoichiometry between the NC and RNP that constitutes a predictable formulation that is considerably smaller than other nonviral Cas9 delivery strategies.

The monomeric precursors of NCs allow for easy fine-tuning of the ratios and amounts of monomers to control endosomal escape and cytosol release of RNP from NCs, as well as the conjugation of functional moieties. This customizability is a key advantage over lipid-based<sup>29</sup> and protein-engineering<sup>30</sup>-based methods which may be less flexible. NCs also retain their biological functions after freeze-drying, thereby allowing for long-term storage and transport. Furthermore, employing protein engineering to facilitate delivery may alter Cas9-sgRNA interactions and interfere with proper RNP function as described previously<sup>30</sup>. Our NC delivery system demonstrated robust gene editing outcomes and lower cytotoxicity. Finally, the NC delivery system also induced efficient gene editing *in vivo*, highlighting its versatility via surface modification. Due to the small size, modularity, and low cytotoxicity of NCs, we anticipate that NCs could be further tailored to efficiently deliver gene editing machinery to a multitude of cell lines *in vitro* and many tissues *in vivo* for somatic gene editing applications.

## Methods

### Materials:

Acrylic acid (AA), N,N,N',N'-tetramethylethylenediamine (TMEDA), acrylate PEG (APEG; 480 Da), bisacrylamide (BAA), 1-vinylimidazole (VI), and ammonium persulfate (APS) were purchased from ThermoFisher Scientific (Fitchburg, WI, USA). Acrylate PEG-NH<sub>2</sub> (APEG-NH<sub>2</sub>; 2 kDa) was acquired from JenKem Technology (Allen, TX, USA). 4-Imidazolecarboxylic acid, all-trans-retinoic acid (ATRA), N-(3-aminopropyl)methacrylamide hydrochloride (APMA), and N,N'-bis(acryloyl)cystamine (BACA) were obtained from Sigma-Aldrich (St. Louis, MO). Acrylate PEG-Mal (APEG-Mal; 2 kDa) was purchased from Creative PEGWorks (Chapel Hill, NC). Cell penetrating peptide (CPP), TAT-Cys (CYGRKKRRQRRR), was synthesized by Genscript (Piscataway, NJ).

### Cell Culture:

The human embryonic kidney (HEK) cell line was maintained on gelatin-A coated plates at passage 10–50 in Dulbecco's modified Eagle medium (DMEM) supplemented with 10% fetal bovine serum (FBS), 2 mM L-Glutamine, and 50 U/mL Penicillin/Streptomycin. WA09 hESCs (WiCell, Madison, WI) were maintained in mTESR medium on Matrigel (WiCell) coated tissue culture polystyrene plates (BD Falcon). hESCs were passaged every 3–4 days at a 1:6 ratio using Versene solution (Life Technologies). H2B-mCherry transgenic lines were generated as previously reported<sup>31</sup> through CRISPR-mediated insertion of an AAV-CAGGS-EGFP plasmid (Addgene #22212), modified to express Histone 2B-mCherry, at the *AAVS1* safe harbor locus using gRNA AAVS1-T2 (Addgene #41818). All cells were maintained at 37 °C and 5% CO<sub>2</sub>. Cell lines were kept mCherry positive through puromycin selection or fluorescence assisted cell sorting (FACS) on a BD FACS Aria.

### sgRNAs *In Vitro* Transcription:

A DNA double stranded template of a truncated T7 promoter and desired sgRNA sequence was formed through overlap PCR using Q5 high fidelity polymerase (New England Biolabs) according to manufacturer's protocols and was placed in the thermocycler for 35 cycles of 98 °C for 5 s, 52 °C for 10 s, and 72 °C for 15 s, with a final extension period of 72 °C for 10 min. PCR products were then incubated overnight at 37°C in a HiScribe T7 *in vitro* transcription reaction (New England Biolabs) according to manufacturer's protocol. The resulting RNA was purified using a MEGAclean Transcription Clean-Up Kit (Thermo Fisher). sgRNA concentration was quantified using a Qubit fluorometer (Thermo Fisher). The sgRNA sequences used were (with PAM site):  
mCherry:GGAGCCGTACATGAACTGAGGGG; APP: ATCCATTCATCATGGTGGTGG;  
tdTomato: AAGTAAAACCTCTACAAATGTGG.

### Preparation of nanocapsules (NCs):

Sodium bicarbonate buffer (10 mM, pH = 9.0) was freshly prepared and degassed using the freeze–pump–thaw method for 3 cycles. sNLS-Cas9-sNLS protein (Aldevron, Madison, WI) was combined with sgRNA at a 1:1 molar ratio and allowed to complex for 5 minutes with gentle mixing. AA, APMA, VI, and APEG were accurately weighed and dissolved in degassed sodium bicarbonate buffer (2 mg/ml). VI, APS, and TMEDA were accurately weighed and dissolved in degassed sodium bicarbonate buffer (1 mg/ml). Cas9 RNP complex was diluted to 0.12 mg/mL in sodium bicarbonate buffer in a nitrogen atmosphere. Monomer solutions were added into the above solution under stirring in the order of AA, APMA, and VI at 5-minute intervals. In each 5-minute interval, the solution was degassed by vacuum pump for 3 minutes and refluxed with nitrogen. After another 5 min, the crosslinker, BACA, was added, followed by the addition of ammonium persulfate. The mixture was degassed for 5 min, and the polymerization reaction was immediately initiated by the addition of TMEDA. After 65 min of polymerization under a nitrogen atmosphere, the APEG was added. The reaction was resumed for another 30 min. Finally, unreacted monomers and initiators were removed by dialysis in 20 mM phosphate-buffered saline (PBS) buffer (pH 7.4). The molar ratio of AA/APMA/VI/BACA/APEG (i/ii/iii/iv/v) used for the optimal formulation was 927/927/244/231/33. The molar ratio of RNP:APS: TMEDA was kept at 1:1:1.

For the preparation of NCs conjugated with CPP (i.e., NC-CPP), we first prepared acrylate PEG-CPP (APEG-CPP) by reacting APEG-Mal and TAT-Cys through an SH-Mal reaction in an aqueous solution at a pH of 7.4. Then, the NC-CPP was prepared following a similar protocol as described above with the molar ratio of AA/APMA/VI/BACA/APEG-CPP at 927/927/244/231/33.

For the preparation of NCs conjugated with all-trans-retinoic acid (ATRA) (i.e., NC-ATRA), acrylate PEG-ATRA (APEG-ATRA) was first prepared by reacting APEG-NHS and ATRA through amidization. Briefly, APEG-NHS (1.0 mg), ATRA (0.18 mg), 1-ethyl-3-(3-dimethylaminopropyl)carbodiimide (0.11 mg), and N-hydroxysuccinimide (0.10 mg) were dissolved in PBS (3 mL; pH 7.4). The solution was stirred at room temperature for 24 h. Subsequently, it was dialyzed against DI water for 48 h to remove impurities. The polymer,

APEG-ATRA, was obtained by lyophilization. Then, the NC-ATRA was prepared following the similar protocol as described above with the molar ratio of AA/APMA/VI/BACA/APEG/APEG-ATRA at 927/927/244/231/33.

The dried NCs were prepared using either a fast or slow freezing process before lyophilization. For the fast freezing process, NC solutions were frozen rapidly using liquid nitrogen and were then dried using a lyophilizer. For the slow freezing process, NC solutions were frozen using a Mr. Frosty™ Freezing Container at a cooling rate of  $-1^{\circ}\text{C}/\text{minute}$  (Thermo Fisher Scientific, Fitchburg, WI) and were then dried using a lyophilizer.

#### Characterization:

The sizes and morphologies of Cas9 RNP NCs were studied by dynamic light scattering (DLS, ZetaSizer Nano ZS90, Malvern Instruments, USA) and transmission electron microscopy (TEM, FEI Tecnai G<sup>2</sup> F30 TWIN 300 KV, E.A. Fischione Instruments, Inc. USA). Zeta potentials were measured by ZetaSizer Nano ZS90 (Malvern Instruments, USA). The RNP loading level and efficiency of NC were determined by the bicinchoninic acid (BCA) assay.

#### Assaying RNP Delivery:

Cells were seeded in 96 well plates in 100  $\mu\text{l}$  of media one day prior to transfection. On the day of transfection, unencapsulated RNP, NC-RNP or Lipofectamine-based RNP complexes (including Lipofectamine 2000/RNP and Lipofectamine CRISPRMAX/RNP) were added to the cells for transfection of RNPs according to manufacturer instructions (e.g., 0.2–0.75  $\mu\text{l}/\text{well}$  of Lipofectamine 2000 and 0.3  $\mu\text{l}/\text{well}$  of Lipofectamine CRISPRMAX). At day 6, cells were collected for flow cytometry (BD FACSCanto II) and assayed for mCherry expression. Flow analysis was performed using FlowJo software. For HEK 293s, 7.8 nM RNP was used per well. To examine the activity of unencapsulated RNP, a high dose (1  $\mu\text{M}$ ) of RNP was also tested.

For experiments involving *APP* targeting, cells were cultured in 24 well plates at 50,000 cells/well. 6.25 nM RNP were used to transfect HEK 293 cells, while 25 nM RNP were used to transfect human embryonic stem cells (hESCs).

To study the stability of the RNP NCs in the presence of GSH, the gene editing efficiency of NCs under different GSH concentrations was tested. The experiments were carried out under similar conditions as described above using GSH-containing media, instead. The GSH concentration investigated ranged from 0 to 20 mM.

#### Genomic analysis:

DNA was isolated from cells using DNA QuickExtract (Epicentre, Madison, WI) following treatment by 0.05% trypsin-EDTA and centrifugation. QuickExtract solution was incubated at 65  $^{\circ}\text{C}$  for 15 min, 68  $^{\circ}\text{C}$  for 15 min, and then 98  $^{\circ}\text{C}$  for 10 min. Genomic PCR was performed following manufacturer's instructions using Q5 High fidelity DNA polymerase (New England Biolabs) and ~500 ng of genomic DNA. Products were then purified using AMPure XP magnetic bead purification kit (Beckman Coulter) and quantified using a

Nanodrop2000 or Qubit (Thermo Fisher). For deep sequencing of the *APP* locus, genomic DNA was amplified using the following primers: TGTCATAGCGACAGTGATCGT and AGCTAAGCCTAATTCTCTCATAGTC. Samples were pooled and run on an Illumina Miniseq with read length of 150bp. Deep sequencing data was analyzed using the Cas-Analyzer software<sup>32</sup>.

#### **Intracellular Trafficking:**

HEK 293 cells were seeded at a density of ~40,000 cells/well one day prior to transfection in 1  $\mu$ m<sup>2</sup> well culture chambers (Ibidi). NCs were formed with Atto-550 fluorescently tagged tracrRNA (Integrated DNA Technologies) combined with crRNA and added to cells at 1  $\mu$ g/well for transfection. After 6 h incubation, cells were stained with LysoTracker Green DND-26 and DAPI for endosomes/lysosomes and nuclei, respectively. Cells were imaged using an Eclipse TI epifluorescent microscope (Nikon) and as AR1 confocal microscope (Nikon). Image analysis was performed using CellProfiler. For flow cytometric analysis, HEK 293 cells were seeded in 96 well plates and dissociated after 4 hours, followed by flow cytometry on an Accuri C6 (BD Biosciences).

#### **MTT Assay:**

HEK 293 cells were seeded in 96 well plates (17,500 cells/well) in 100  $\mu$ l of media one day prior to transfection. On the day of transfection, NC, RNP/Lipofectamine 2000 (0.2–0.75  $\mu$ l/well), or RNP/Lipofectamine CRISPRMAX (0.3  $\mu$ l/well) were added to the cells. After two day of incubation, a standard MTT assay was performed by aspirating the treatment media, adding 25  $\mu$ L of the medium containing 0.5mg/mL MTT agent, and incubating at 37  $^{\circ}$ C for 4 h. Thereafter, the medium was aspirated and 75  $\mu$ L of DMSO was added to each well. The plates were then measured at 570 nm using a spectrophotometer (Quant, Bio-Tek Instruments, Winooski, VT), and the average absorbance and percent of cell viability relative to the control (pure medium) were calculated.

#### **Subretinal Injection:**

For mice studies, Ai14 mice (obtained from Jackson Labs) were used to assay gene editing efficiency in retinal pigment epithelium (RPE). All RNPs were formed with sgRNA targeted for excision of SV40 polyA blocks<sup>22</sup> (target sequence: AAGTAAAACCTCTACAAATG). As previously described, mice were maintained under tightly controlled temperature (23  $\pm$  5  $^{\circ}$ C), humidity (40–50%) and light/dark (12/12 h) cycle conditions in 200 lux light environment. The mice were anesthetized by intraperitoneal injection of ketamine (80 mg/kg), xylazine (16 mg/kg) and acepromazine (5 mg/kg) cocktail. Prior to the sub-retinal injection, the cornea was anesthetized with a drop of 0.5% proparacaine HCl and the pupil was dilated with 1.0% tropicamide ophthalmic solution (Bausch & Lomb Incorporated, Rochester, NY). Thermal stability was maintained by placing mice on a temperature-regulated heating pad during the injection and for recovery purposes. All surgical manipulations were carried out under a surgical microscope (AmScope, Irvine, CA). 2  $\mu$ L of solution containing either RNP alone, NC, or NC-ATRA, at the concentration of 8  $\mu$ g RNP was injected into the sub-retinal space using the UMP3 ultramicro pump fitted with a NanoFil syringe, and the RPE-KIT (all from World Precision Instruments, Sarasota, FL) equipped with 34 gauge beveled needle. Successful administration was confirmed by bleb

formation (Fig. S5). The tip of the needle remained in the bleb for 10 s after bleb formation, when it was gently withdrawn. A solution (2  $\mu$ L) of PBS vehicle was also injected into the sub-retinal space of the contralateral eye to serve as a control.

To assess tdTomato expression generated by successful gene editing, the mice were sacrificed, and eyes were collected 12 days after injection. Eucleated eyes from the sacrificed mice were rinsed twice with PBS, a puncture was made at ora serrata with an 18 gauge needle and the eyes were opened along the corneal incisions. The lens was then carefully removed. The eye cup was flattened making incisions radially to the center giving the final “starfish” appearance. The retina was then separated gently from the RPE layer. The separated RPE and retina were flat mounted on the cover-glass slide and were imaged with NIS-Elements using a Nikon C2 confocal microscope (Nikon Instruments Inc., Mellville, NY). 561 nm Diode Lasers for red excitation was used to evaluate the tdTomato expression in the RPE layer and images were captured by Low Noise PMT C2 detectors in a Plan Apo VC 20X/0.75, 1 mm WD lens. ImageJ (NIH) was used for image analysis to measure the tdTomato positive areas in relevant ROIs (masked to RPE areas from brightfield images).

#### **Intramuscular injection:**

All treatments (PBS, RNP, and NC) were administered to adult mice *via* the tibialis anterior (TA, 8–10  $\mu$ L per muscle) using a 33-gauge needle with a Hamilton syringe. Twelve days after the injection, TA muscles were harvested and flash-frozen in super-cooled isopentane. TA muscles were then sectioned at 20  $\mu$ m using a cryostat and placed on glass slides. After mounting a slide glass, muscle sections were observed with by using a Keyence BZ-X710 fluorescence microscope (Osaka, Japan) to visualize tdTomato fluorescence. For quantification of fluorescence signals, three sections per muscle were selected from the similar locations in the TA muscle. The relative intensity of tdTomato-positive signal was densitometrically evaluated using NIH ImageJ software.

For immunohistochemistry, the muscle sections were fixed with 4% paraformaldehyde-phosphate-buffered saline, and then incubated with primary antibodies for overnight. The following primary antibodies were used to probe for muscle satellite cells and tdTomato, respectively: anti-Pax7 (Developmental Studies Hybridoma Bank, Iowa City, IA) and anti-RFP (rabbit polyclonal, Rockland Immunochemical Inc., Limerick PA). The primary antibodies were then detected by fluorescence-conjugated secondary antibodies. All images were optimized by using a Nikon Eclipse 80i fluorescence microscope with a digital camera (DS-QiIMC, Nikon, Tokyo, Japan).

## **Supplementary Material**

Refer to Web version on PubMed Central for supplementary material.

## **Acknowledgements**

We thank the James Thomson lab for the use of their BD FACSCanto II, and the University of Wisconsin Biotechnology Center for providing facilities and services. We thank Aldevron for supplying reagents and technical support. We are grateful to Prof. Qiang Chang who provided us with the Ai14 tdTomato transgenic mice used for

initial evaluation. We acknowledge the generous financial support from the National Institute for Health (UG3 TR002659-01, R01EY024995, 1R35GM119644, R01NS091540, R01HL143469, and R01 HL129785), the National Science Foundation (CBET-1350178 and CBET-1645123), the Wisconsin Alumni Research Foundation, and the Wisconsin Institute for Discovery. The authors would also like to acknowledge financial support from the University of Wisconsin–Madison.

## References

1. Yin H, Kauffman KJ & Anderson DG Delivery technologies for genome editing. *Nat. Rev. Drug Discov* 16, 387–399 (2017). [PubMed: 28337020]
2. Liu J et al. Efficient delivery of nuclease proteins for genome editing in human stem cells and primary cells. *Nat. Protoc* 10, 1842–1859 (2015). [PubMed: 26492140]
3. Li L, He Z, Wei X, Gao G & Wei Y Challenges in CRISPR/CAS9 delivery: potential roles of nonviral vectors. *Hum. Gene Ther* 26, 452–462 (2015). [PubMed: 26176432]
4. Mout R, Ray M, Lee YW, Scaletti F & Rotello VM In vivo delivery of CRISPR/Cas9 for therapeutic gene editing: progress and challenges. *Bioconjugate Chem* 28, 880–884 (2017).
5. Wang HX et al. CRISPR/Cas9-based genome editing for disease modeling and therapy: challenges and opportunities for nonviral delivery. *Chem. Rev* 117, 9874–9906 (2017). [PubMed: 28640612]
6. Li L, Hu S & Chen X Non-viral delivery systems for CRISPR/Cas9-based genome editing: Challenges and opportunities. *Biomaterials* 171, 207–218 (2018). [PubMed: 29704747]
7. Rui Y, Wilson DR & Green JJ Non-viral delivery to enable genome editing. *Trends Biotechnol* 37, 281–293 (2019). [PubMed: 30278987]
8. Gu Z et al. Protein nanocapsule weaved with enzymatically degradable polymeric network. *Nano Lett* 9, 4533–4538 (2009). [PubMed: 19995089]
9. Zhao M et al. Clickable protein nanocapsules for targeted delivery of recombinant p53 protein. *J. Am. Chem. Soc* 136, 15319–15325 (2014). [PubMed: 25289975]
10. Yan M, et al. A novel intracellular protein delivery platform based on single-protein nanocapsules. *Nat. Nanotechnol* 5, 48–53 (2010). [PubMed: 19935648]
11. Putnam D, Gentry CA, Pack DW & Langer R Polymer-based gene delivery with low cytotoxicity by a unique balance of side-chain termini. *Proc. Natl Acad. Sci. USA* 98, 1200–1205 (2001). [PubMed: 11158617]
12. Meng F, Cheng R, Deng C & Zhong Z Intracellular drug release nanosystems. *Mater. Today* 15, 436–442 (2012).
13. Liu F et al. PKM2 methylation by CARM1 activates aerobic glycolysis to promote tumorigenesis. *Nat Cell Biol* 19, 1358–1370 (2017). [PubMed: 29058718]
14. Mout R et al. Direct cytosolic delivery of CRISPR/Cas9-ribonucleoprotein for efficient gene editing. *ACS Nano* 11, 2452–2458 (2017). [PubMed: 28129503]
15. Carlson-Stevermer J et al. High-content analysis of CRISPR-Cas9 gene-edited human embryonic stem cells. *Stem Cell Rep* 6, 109–120 (2016).
16. Carlson-Stevermer J et al. Assembly of CRISPR ribonucleoproteins with biotinylated oligonucleotides via an RNA aptamer for precise gene editing. *Nat. Commun* 8, 1711 (2017). [PubMed: 29167458]
17. Elzes MR, Akeroyd N, Engbersen JF & Paulusse JM Disulfide-functional poly (amido amine)s with tunable degradability for gene delivery. *J. Control. Release* 244, 357–365 (2016). [PubMed: 27565216]
18. Staahl BT et al. Efficient genome editing in the mouse brain by local delivery of engineered Cas9 ribonucleoprotein complexes. *Nat. Biotechnol* 35, 431–434 (2017). [PubMed: 28191903]
19. Payton NM, Wempe MF & Xu Y Anchordoquy TJ. Long-term storage of lyophilized liposomal formulations. *J. Pharm. Sci* 103, 3869–3878 (2014). [PubMed: 25308534]
20. Chen G et al. Multi-functional self-fluorescent unimolecular micelles for tumor-targeted drug delivery and bioimaging. *Biomaterials* 47, 41–50 (2015). [PubMed: 25682159]
21. Sun J et al. CRISPR/Cas9 editing of APP C-terminus attenuates  $\beta$ -cleavage and promotes  $\alpha$ -cleavage. *Nat. Commun* 10, 53 (2019). [PubMed: 30604771]

22. Berger W, Kloeckener-Gruissem B & Neidhardt J The molecular basis of human retinal and vitreoretinal diseases. *Prog. Retin. Eye Res* 29, 335–375 (2010). [PubMed: 20362068]
23. Maeder ML et al. Development of a gene-editing approach to restore vision loss in Leber congenital amaurosis type 10. *Nat. Med* 25, 229–233 (2019). [PubMed: 30664785]
24. Sun D et al. Targeted multifunctional lipid ECO plasmid DNA nanoparticles as efficient non-viral gene therapy for leber's congenital amaurosis. *Mol. Ther. Nucleic Acids* 7, 42–52 (2017). [PubMed: 28624218]
25. Marmor MF Control of subretinal fluid: experimental and clinical studies. *Eye* 4, 340–344 (1990). [PubMed: 2199242]
26. Strauss O The retinal pigment epithelium in visual function. *Physiol. Rev* 85, 845–881 (2005). [PubMed: 15987797]
27. Mao Y & Finnemann SC Analysis of photoreceptor outer segment phagocytosis by RPE cells in culture. *Retinal Degeneration Springer*, pp 285–295 (2012).
28. Mazzoni F, Mao Y & Finnemann SC Advanced Analysis of Photoreceptor Outer Segment Phagocytosis by RPE Cells in Culture. *Retinal Degeneration Springer*, 2019, pp 95–108.
29. Steyer B et al. High content analysis platform for optimization of lipid mediated CRISPR-Cas9 delivery strategies in human cells. *Acta Biomater* 34, 143–158 (2016). [PubMed: 26747759]
30. Zuris JA et al. Cationic lipid-mediated delivery of proteins enables efficient protein-based genome editing in vitro and in vivo. *Nat Biotechnol* 33, 73–80 (2015). [PubMed: 25357182]
31. Harkness T et al. High-content imaging with micropatterned multiwell plates reveals influence of cell geometry and cytoskeleton on chromatin dynamics. *Biotechnol. J* 10, 1555–1567 (2015). [PubMed: 26097126]
32. Park J, Lim K, Kim JS & Bae S Cas-analyzer: an online tool for assessing genome editing results using NGS data. *Bioinformatics* 33, 286–288 (2017). [PubMed: 27559154]



value of the same component in the optimal formulation. Data are presented as mean  $\pm$  SD (n= 3). **d**, Transmission electron microscope (TEM) images of NCs. Experiments were repeated three times. **e**, Dynamic light scattering (DLS) plots of NCs. Experiments were repeated three times. **f**, Summary of the size and zeta potential of Cas9 protein, Cas9 RNP, and NC. Data are presented as mean  $\pm$  SD (n= 3). Statistical significance was calculated via one-way ANOVA with a Tukey post-hoc test. \* $P < 0.05$ , \*\* $P < 0.01$ , \*\*\* $P < 0.001$ .

Author Manuscript

Author Manuscript

Author Manuscript

Author Manuscript

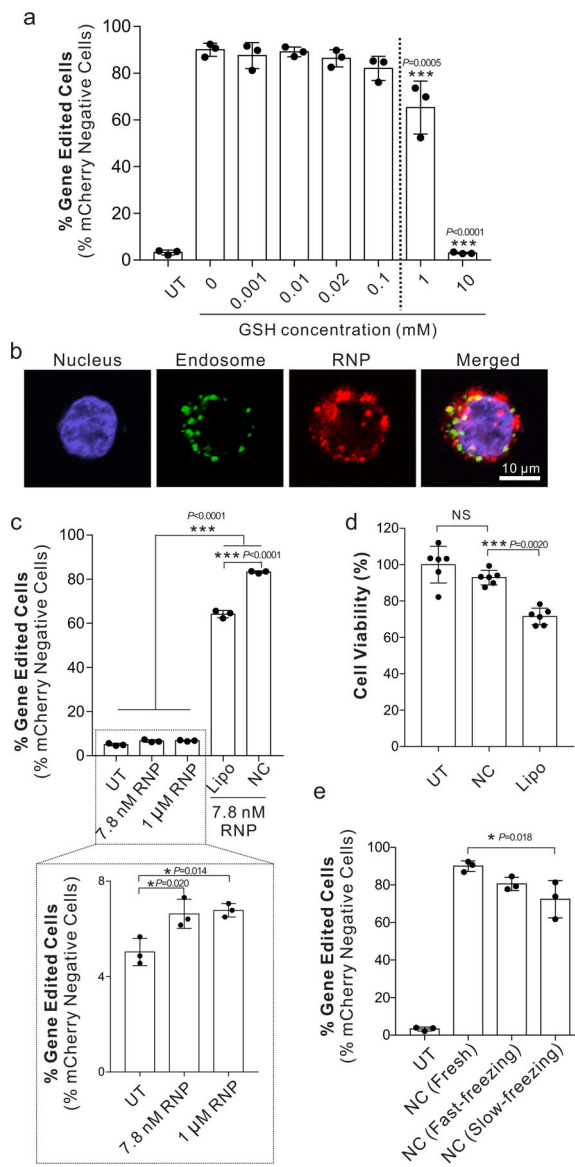


**Figure 2 | Stability, uptake, and toxicity characteristics of NCs within human cells *in vitro*.**

**a**, Stability and responsiveness study of NCs with different concentrations of GSH. Gene editing efficiencies of NCs in GSH-containing media were tested in mCherry-HEK cells with an sgRNA targeting mCherry. The loss of mCherry fluorescence was measured six days after transfection via flow cytometry to assay editing efficiency. Data are presented as mean  $\pm$  SD ( $n=3$ ). **b**, Intracellular distribution of NCs in HEK cells using confocal laser scanning microscopy (CLSM) 6 hours after transfection. The sgRNA was covalently labeled with the ATTO-550 fluorophore (red signal) to track its intracellular location. Cells were stained with LysoTracker Green DND-26 and DAPI for endosomes/lysosomes and nuclei, respectively. Scale bar: 10  $\mu$ m. Experiments were repeated three times. **c**, Gene editing in mCherry-HEK293 cells with unencapsulated RNP, optimized Lipofectamine 2000 system (i.e., Lipo), or NC. Data are presented as mean  $\pm$  SD ( $n=3$ ). **d**, Cell viability measured by an MTT assay after treatment with Lipo and NCs. Data are presented as mean  $\pm$  SD ( $n=6$ ). **e**, Editing

efficiency of NCs after lyophilization. Treatments included freshly prepared NCs [i.e., NC (Fresh)], NCs lyophilized after a fast-freezing process [i.e., NC (Fast-freezing lyophilization)], or NCs lyophilized after a slow freezing process (i.e., NC (Slow-freezing lyophilization)). Data are presented as mean  $\pm$  SD (n= 3). Statistical significance was calculated via one-way ANOVA with a Tukey post-hoc test. \* $P < 0.05$ , \*\* $P < 0.01$ , \*\*\* $P < 0.001$ .

Author Manuscript

Author Manuscript

Author Manuscript

Author Manuscript

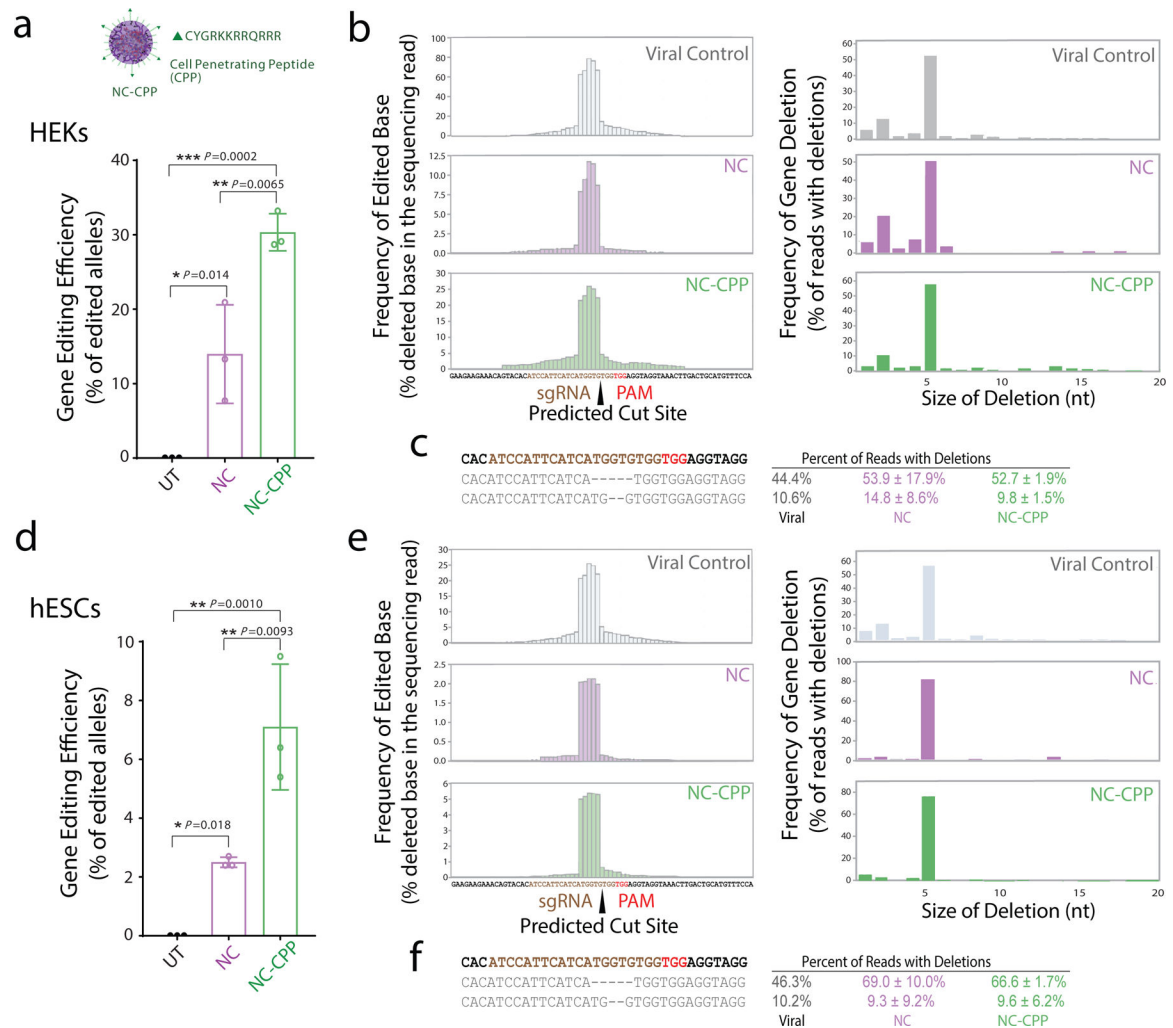


**Figure 3 | Decoration of NCs with targeting ligands increases on-target genome editing efficiency *in vitro* within human cell lines.**

**a**, Deep sequencing of human embryonic kidney (HEK) cells transfected with NCs containing a Cas9 RNP with an sgRNA targeting the endogenous *APP* locus. NCs were decorated with cell-penetrating peptides (NC-CPP). Targeted PCR amplification around the on-target site reveals high on-target editing by NCs. Percent of sequencing reads with a genomic edit are plotted compared to an untransfected control sample (UT). Data are presented as mean ± SD (n=3). **b**, Deletion spectra for reads with deleted bases are shown for every base proximal to the sgRNA target. Viral control refers to previously characterized spectrum for this sgRNA in HEK cells from Sun *et al.*<sup>21</sup> Figures on the right show the size of deletions in the edited sequencing reads. **c**, Frequencies of major reads with deletions in HEK cells. Data are presented as mean ± SD (n=3). **d**, Deep sequencing of human embryonic stem cells (hESCs) transfected with NCs containing a Cas9 RNP with an sgRNA targeting the endogenous *APP* locus. Data are presented as mean ± SD (n=3). **e**, Deletion spectra and size of deletions in hESCs as noted in **b**. **f**, Frequencies of major reads with deletions in hESC cells. Data are presented as mean ± SD (n=3). Statistical significance was

calculated via one-way ANOVA with a Tukey post-hoc test. \* $P < 0.05$ , \*\* $P < 0.01$ , \*\*\* $P < 0.001$ .

Author Manuscript

Author Manuscript

Author Manuscript

Author Manuscript

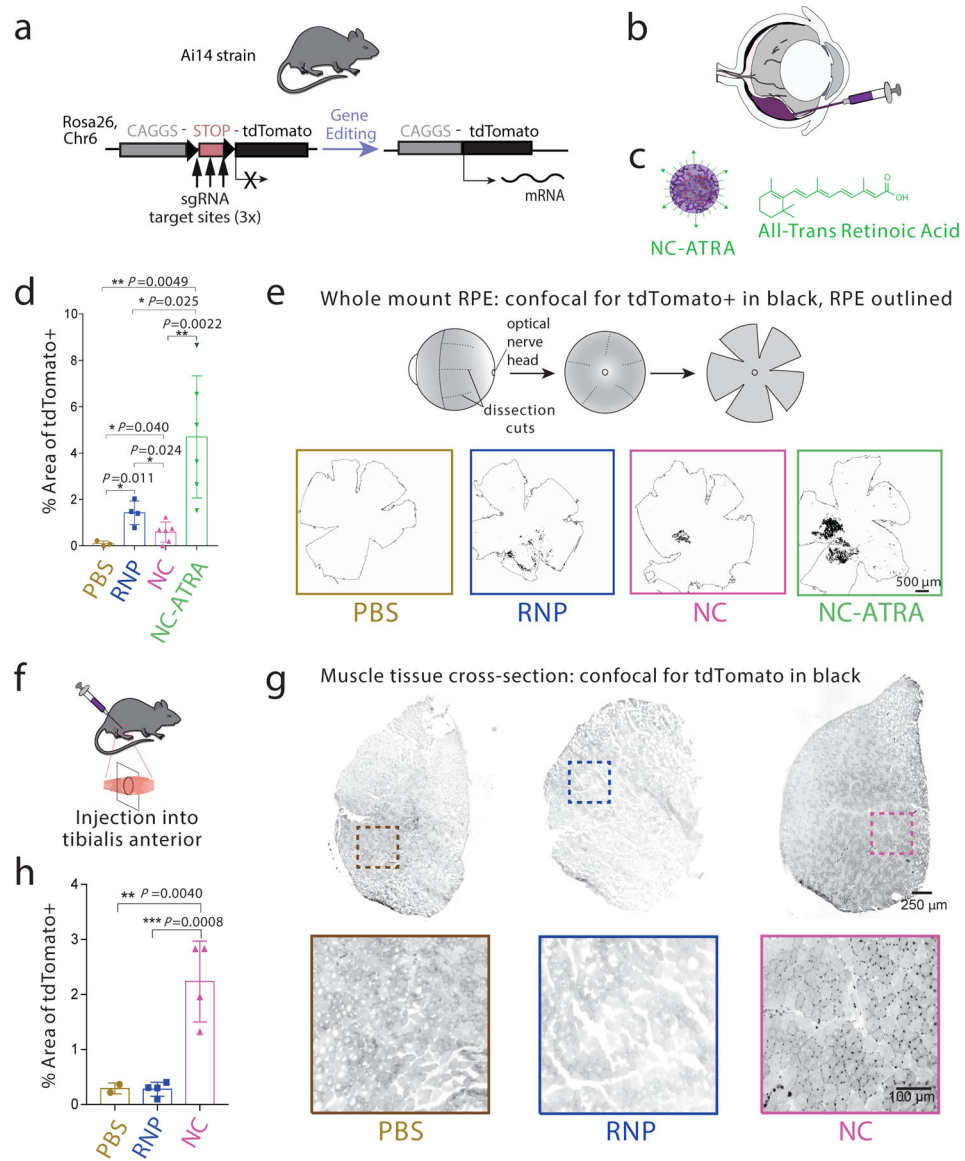


**Figure 4 | NCs can induce efficient genome editing *in vivo* within Ai14 reporter mice.**  
**a**, Schematic of the tdTomato locus within the Ai14 mouse strain. A STOP cassette consisting of three SV40 polyA sequences prevents transcription of the downstream red fluorescent protein variant, tdTomato (left). When cells are edited by CRISPR/Cas9 to excise the STOP cassette via cut sites present in each of the repeats, they will express tdTomato (right). **b**, Schematic of the subretinal injection of genome editors to target the retinal pigmented epithelium (RPE) cells. **c**, Illustration of NC-ATRA. **d**, Genome editing efficiency as quantified by percent of area of whole RPE with genome editing reporter (tdTomato+). PBS (n=3), RNP (n=4), NC (n=6), or NC-ATRA (n=6). Data are presented as mean ± SD. **e**, Schematic of whole mount RPE preparation and representative images of tdTomato+ signal (black) 12 d after subretinal injection. The whole RPE layer is outlined. Experiments were repeated three times. **f**, Schematic of intramuscular injection of genome editors. **g**, Representative images of the muscle tissues 12 days after intramuscular injection

of either PBS, RNP, or NC. Experiments were repeated three times. **h**, Gene editing efficiency as quantified by percent of area of whole muscle tissue with genome editing reporter (tdTomato+). n=4 for all conditions except PBS (n=2). Data are presented as mean  $\pm$  SD. Statistical significance was calculated via one-way ANOVA with a Tukey post-hoc test. \* $P < 0.05$ , \*\* $P < 0.01$ , \*\*\* $P < 0.001$ .

Author Manuscript

Author Manuscript

Author Manuscript

Author Manuscript